Available online at www.sciencedirect.com
ScienceDirect
Catalysis Today 131 (2008) 226–237
CATALYSIS TODAY
www.elsevier.com/locate/cattod

Effect of complex oxide promoters and Pd on activity and stability of Ni/YSZ (ScSZ) cermets as anode materials for IT SOFC

Vladislav A. Sadykov [a,*], Natalia V. Mezentseva [a], Rimma V. Bunina [a], Galina M. Alikina [a], Anton I. Lukashevich [a], Tamara S. Kharlamova [a], Vladimir A. Rogov [a], Vladimir I. Zaikovskii [a], Arcady V. Ishchenko [a], Tamara A. Krieger [a], Oleg F. Bobrenok [b], Alevtina Smirnova [c], John Irvine [d], Oleksandr D. Vasylyev [e]

[a] *Boreskov Institute of Catalysis SB RAS, Novosibirsk, Russian Federation*
[b] *Institute of Thermophysics SB RAS, Novosibirsk, Russian Federation*
[c] *Global Fuel Cells Center, University of Connecticut, Storrs, CT, USA*
[d] *School of Chemistry, University of St. Andrews, Fife, United Kingdom*
[e] *Institute for Problems of Materials Science, Kiev, Ukraine*

Available online 26 November 2007

Abstract

Effect of fluorite-like or perovskite-like complex oxide promoters, Pd and Cu on the performance of Ni/8YSZ and Ni/ScCeSZ anode materials in CH_4 steam reforming (SR) or selective oxidation (SO) by O_2 into syngas was studied. The spatial distribution of dopants in composites before and after contact with the reaction feed, features of components mutual interaction and forms of deposited coke were controlled by TEM combined with EDX analysis. The lattice oxygen mobility and reactivity were estimated by CH_4 and H_2 temperature-programmed reduction (TPR), and the amount of deposited carbon after operation in the feed with stoichiometric H_2O/CH_4 ratio was estimated by the temperature-programmed oxidation. Promoters decrease the amount of deposited coke, while doping by Pd or Cu ensures also a good and stable performance at moderate (~550 °C) temperatures required for the intermediate-temperature solid oxide fuel cells (IT SOFC) operation.

Keywords: SOFC composite anodes; Methane steam reforming; Promoters; Microstructure; TEM; EDX; H_2 and CH_4 TPR

1. Introduction

Design of anode materials for solid oxide fuel cells (SOFC) operating at intermediate temperatures (IT) in methane/steam feeds without coking represents important but demanding problem [1]. State-of-the art $Ni/Y_2O_3–ZrO_2$ (Ni/YSZ) cermet anodes have excellent catalytic properties and stability for the H_2 oxidation at SOFC operation conditions [2,3]. However, the lack of a hydrogen infrastructure and the unsolved hydrogen storage problem have initiated the research aimed at direct utilization of natural gas, which represents one of the key aspects of SOFC technology. Internal steam reforming (SR) is the most promising concept in using the natural gas as a fuel [3,4]. In this case, the reaction takes place directly in the anode compartment, allowing a better management of heat within the stack. Unfortunately, with the cermet Ni/YSZ anode, coking occurs leading to the deterioration of anode performance [2,4]. Hence, development of robust anode materials with a high and stable activity in the SR of hydrocarbon fuels is vital for the natural gas fuel-based SOFC. Next approaches were suggested up to date to solve this problem:

1. Partial or complete replacement of doped zirconia with doped ceria or ceria–zirconia possessing a higher lattice oxygen mobility/reactivity [2–9]. This is combined with partial or complete replacement of Ni by copper [2,3,10,11]. These anode materials are resistant to coking and possess a high performance in SR at intermediate temperatures

* Corresponding author.
E-mail address: sadykov@catalysis.ru (V.A. Sadykov).

0920-5861/$ – see front matter © 2007 Elsevier B.V. All rights reserved.
doi:10.1016/j.cattod.2007.10.064

required for operation of SOFC with doped ceria or gallate-type electrolytes.
2. Replacing doped zirconia by complex perovskites (mainly, complex chromites) with their doping by metals active in SR (Ni or precious metals, mainly, Ru) [12–16].
3. Partial or complete replacement of Ni by precious metals in cermets with complex perovskites [16] or doped zirconia [17–19] as oxide phases. This allows to suppress coking and enhance middle-temperature performance which is explained by a much higher specific catalytic activity of precious metals as compared with Ni in CH_4 SR, Pt being the most active metal [20].

Apart from a high and stable activity in SR in stoichiometric methane/steam feeds, anode materials are to be inexpensive, compatible with electrolytes by the thermal expansion coefficients, possess a high electronic conductivity and phase/mechanical stability to redox cycles [1,3]. For IT SOFC with thin layers of anode-supported Y- or Sc-stabilized zirconia electrolytes considered now as the most promising trend in SOFC design for wide-scale application [21], these set of requirements can be met by using as anode materials Ni/YSZ (ScCeSZ) cermets doped by fluorite-like (ceria or ceria–zirconia) or perovskite-like (complex chromates–manganites) oxides promoted by precious metals or Cu. However, systematic studies regarding effects of such systems composition and preparation routes on their performance in the SR of methane in stoichiometric feeds are not reflected in literature, which hampers optimization of their composition.

This paper presents the experimental results related to the synthesis of these complex Ni-containing anode materials, characterization of their microstructural features and catalytic properties in methane SR in regard of the nature of electrolyte (YSZ or ScCeSZ), type of complex oxide dopant (fluorite- or perovskite-like complex oxide), nature of promoter able to activate methane (Pd or Cu) and composites preparation route. Selection of complex oxide promoters used in this work was based on previous detailed studies of their oxygen mobility and reactivity as related to catalysis of CH_4 transformation into syngas via selective oxidation, autothermal and steam reforming [12,14,22–31]. Since the primary aim of this research is to select the most promising compositions and preparation procedures, at this stage, catalytic performance stability was estimated for relatively short (tens of hours) time-on-stream, since longer tests (including those with anodes in real single-cell tests) are to be carried out later for optimized systems.

2. Experimental

Three types of composite powders were used in this study. The composite I was prepared from 60 wt.% NiO (Novamet, US) and 40% $Sc_{0.1}Ce_{0.01}Zr_{0.89}O_{2-y}$ (DKKK, Japan) powders. Thoroughly mixed powders were pressed into pellets, sintered at 1200 °C for 2 h, crushed and ball milled to micron-sized powders as described earlier [22] resulting in the specific surface area (S_{sp}) of ~1 m^2/g.

Composite II (S_{sp}, 5 m^2/g) was comprised of the mixture of NiO (60 wt.%) and $Y_{0.08}Zr_{0.92}O_{2-y}$ (8YSZ, Russian sources) mixed and ball milled followed by the powders calcinations at 900 °C for 2 h [23].

Composites I and II were doped with fluorite ($Pr_{0.02}Gd_{0.18}Ce_{0.8}O_{2-y}$, $Gd_{0.2}Ce_{0.8}O_{2-y}$ and $Ce_{0.5}Zr_{0.5}O_{2-y}$) or perovskite ($La_{0.8}Pr_{0.2}Mn_{0.2}Cr_{0.8}O_3$) oxides (loading 3 wt.% for composite I and 10 wt.% for composite II) by impregnation with aqueous solutions of polyester citric acid–ethylene glycol precursors prepared as described elsewhere [24] followed by drying and calcinations at 700 °C for 4 h. Detailed characterization of the structural and surface characteristics of these dopants as related to their surface/lattice oxygen mobility and reactivity is given in previous publications [12,14,22–31].

Doped composite III (S_{sp}, 23 m^2/g) was comprised of 55% NiO, 35% of nanocrystalline $Sc_{0.1}Ce_{0.01}Zr_{0.89}O_{2-y}$ electrolyte prepared via coprecipitation route as described elsewhere [32] and 10 wt.% of complex perovskite-like oxide $La_{0.8}Sr_{0.15}Pr_{0.05}Mn_{0.2}Cr_{0.8}O_{3+x}$. This composite was prepared in one-pot synthesis by dispersing electrolyte powder in the water solution of Ni nitrate and polyester citric acid–ethylene glycol polymeric precursor of a complex perovskite, evaporation of this mixture, decomposition of formed solid residue under air with final calcinations at 700 °C for 4 h. This preparation procedure favors a high dispersion of components in the composite along with their strong chemical interaction apparently exceeding that in more traditional impregnation route used for the preparation of composite I.

Pd (0.3 wt.%) or CuO (10 wt.%) were supported on complex oxides doped composites by incipient wetness impregnation with $PdCl_2$ or $Cu(NO_3)_2$ solutions followed by drying and calcinations at 700 °C for 2 h.

Samples were characterized by X-ray diffraction (XRD), transmission electron microscopy (TEM) and BET surface area analysis.

The XRD patterns were obtained with an URD-6 diffractometer (Germany) using Cu Kα radiation in the 2θ range 5–90°.

The TEM micrographs were obtained with a JEM-2010 instrument (lattice resolution 1.4 Å) and acceleration voltage 200 kV. Local elemental analysis was performed with EDX method (a Phoenix Spectrometer).

The BET specific surface area was determined from the Ar thermal desorption data.

The temperature-programmed reactions of samples reduction (TPR) by H_2 or CH_4 (1% H_2 in Ar or 1% CH_4 in He), deposited coke oxidation (TPO) by O_2 (1% O_2 in He), CH_4 oxidation by O_2 (1% CH_4 + 0.5% O_2 in He), CH_4 SR (1% CH_4 + 1% H_2O in He) were studied in flow installations equipped with quartz reactors, GC and PEM-2 M gas analyzers under the temperature ramp of 5 °C/min up to 880 °C as described elsewhere [24,29]. The steady-state activity of samples in CH_4 SR was studied using more concentrated (8% CH_4 + 8–24% H_2O in N_2) feeds. For TPO experiments, samples after standard pretreatment in oxygen were kept for 3 h in the flow of stoichiometric reaction feed 8% CH_4 + 8% H_2O in N_2, steady-state performance being achieved within 1 h. Samples were then cooled in the same feed to room temperature

within ~3 h, discharged from the reactor and transferred into another one under contact with air for TPO run.

3. Results and discussion

3.1. Structural characteristics and microstructure of composites

3.1.1. "Green" composites

Typical X-ray diffraction patterns for complex oxide composites are shown in Figs. 1 and 2. Along with strong reflections corresponding to doped zirconia and NiO phases [32–34], weak broad reflections corresponding to doping fluorite-like phase (PDF#02-1334) or complex perovskite phase (PDF#89-8771) were observed. Smaller particle sizes (a higher dispersion) of ScCeSZ and NiO in the composite III as compared with composites I and II are reflected in broader diffraction lines of these phases. While reflections corresponding to supported Pd are not observed due to its low content beyond sensitivity of XRD method, reflections corresponding to CuO phase (PDF#801916) are well developed indicating its rather good crystallinity.

Microstructural features of different composites studied by TEM vary strongly. Particles of composite I are comprised of sintered domains of NiO and ScCeSZ (Fig. 3). For doped zirconia, a variation of the lattice spacing corresponding to the (1 1 1) planes from 3.0 Å to 3.2 Å was observed suggesting spatial variation of dopants content in the electrolyte particles [32]. For NiO [*R*-3*m* space group, PDF#44-1159], the (1 0 1) lattice spacing (2.4 Å) was mainly observed. A coherent stacking of NiO and doped zirconia regions (Fig. 3) implies a strong chemical interaction between these phases in sintered composite.

Composite II (Fig. 4) is comprised of separate bulky rounded NiO particles and 8YSZ aggregates with a rather good crystallinity, without any apparent interaction between these oxide phases.

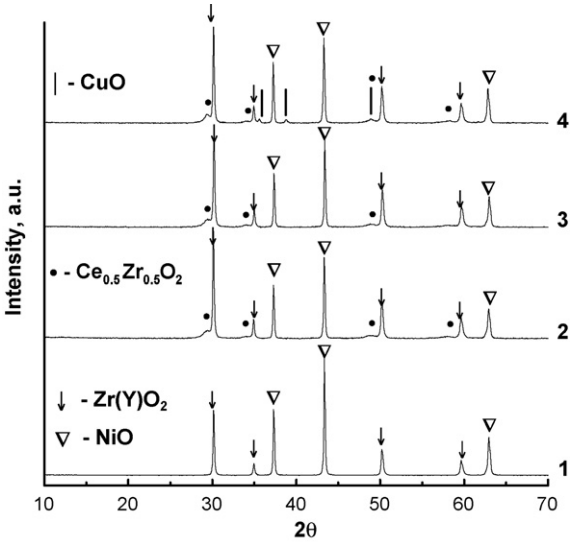

Fig. 1. X-ray diffraction patterns for composite II undoped (1) or doped with: 10 wt.% $Ce_{0.5}Zr_{0.5}O_{2-y}$ (2), 0.3 wt.% Pd + 10 wt.% $Ce_{0.5}Zr_{0.5}O_{2-y}$ (3) and 10 wt.% CuO + 10 wt.% $Ce_{0.5}Zr_{0.5}O_{2-y}$ (4).

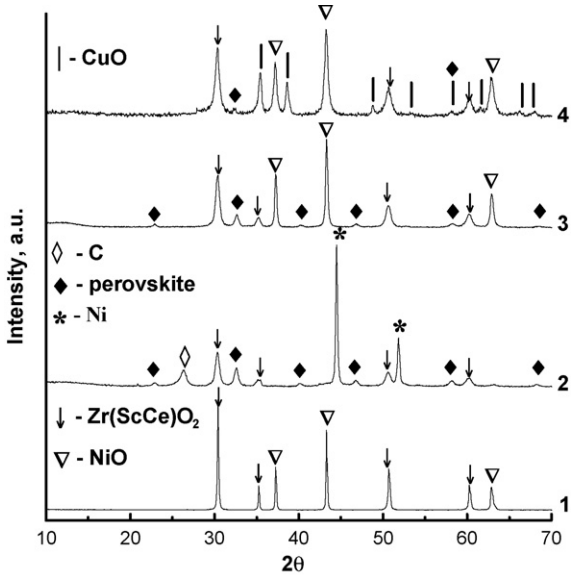

Fig. 2. X-ray diffraction patterns for composites I and III. (1) Composite I, (2) composite III after methane steam reforming (3) composite III doped with 0.3 wt.% Pd and (4) composite III doped with 10 wt.% CuO.

Composite III (Fig. 5) is comprised of loose micron-size aggregates of nanoparticles with pronounced spatial variation of their composition as revealed by EDX. In this system, particles of NiO and perovskite-like phase possessing rather good crystallinity are stacked nearly coherently. Here, for NiO (Fig. 6) distances of 2.1 Å and 2.4 Å corresponding to the (2 0 0) and (1 1 1) planes of *Fm*3*m* (PDF#47-1049) space group are revealed. Distances 3.8 Å, 1.9 Å and 2.8 Å found for particles of $LnCrMnO_3$ phase (*Pbnm* space group, PDF#89-8771) correspond to (1 1 0), (2 2 0) and (2 0 0) planes. In Fig. 6, the interphase boundary (a–c) corresponds to the ideally matched (1 0 0) $LnCrMnO_3$ and (1 1 1) NiO planes (zero angle of distortion), while the boundary (b and c) corresponds to stacking of (1 1 0) $LnCrMnO_3$ and (0 0 2) NiO planes with the angle of distortion equal to 5.3°. A perovskite-like phase is also present as rather disordered regions situated between the NiO particles (Fig. 7).

For composites I and II, complex oxide dopants were mainly present as the surface layers on NiO particles revealed by EDX and typical moiré fringes caused by overlapping lattices of fluorite-like/perovskite-like and NiO phases [23].

For Pd-doped sample of composite II containing the perovskite oxide promoter, separate Pd nanoparticles were observed on the surface of NiO particles [23]. In these particles, a thick PdO shell (lattice spacings 3.1 Å) covers the Pd^0 core (lattice spacings 2.2 Å).

For composites co-doped with fluorite-like oxides and Pd, separate Pd particles were not revealed implying a stronger interaction of Pd oxidic species with these dopants as compared with the perovskite-like oxide.

Hence, microstructural studies revealed pronounced chemical interaction between components in doped composite anode materials, the most pronounced effects being observed for composite III.

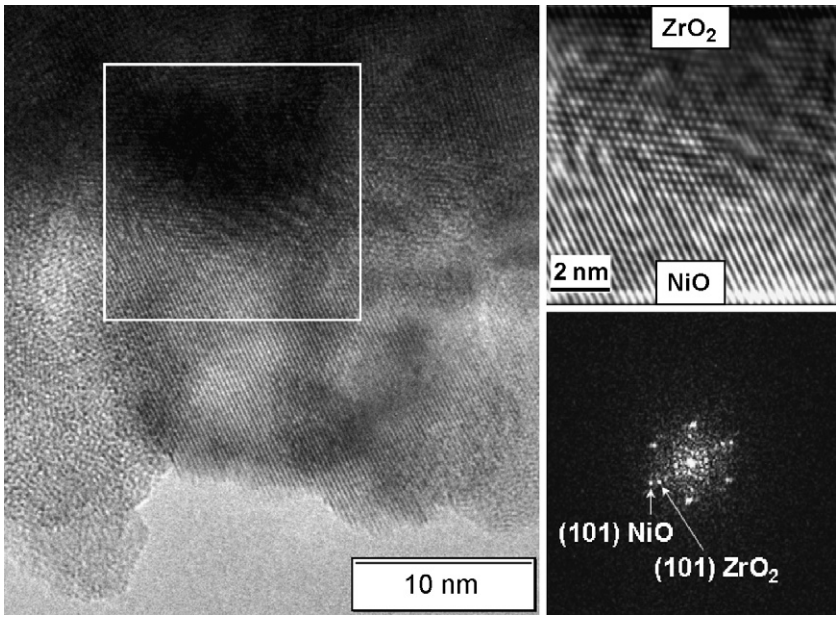

Fig. 3. TEM micrograph of composite I particle with a high resolution image of the intergrown NiO and ZrO_2 lattices and digital diffraction pattern (DDP) from this region.

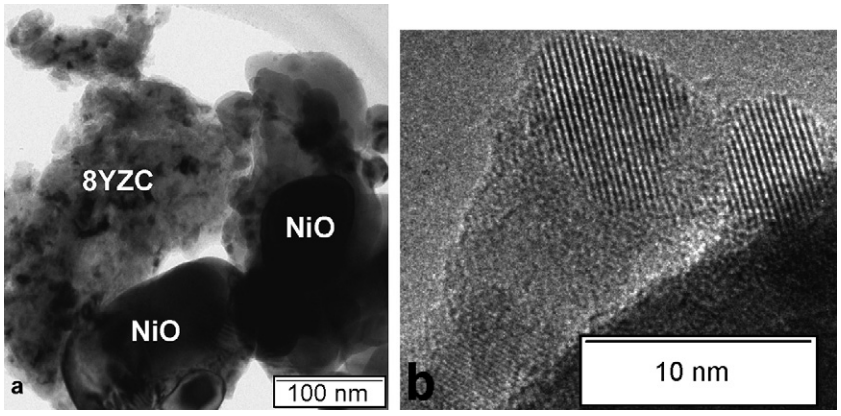

Fig. 4. (a) Typical image of composite II particles and (b) high resolution image of Y-doped zirconia particle lattice with $d_{(1\,0\,1)}$ = 3.0 Å (PCPDF#371307).

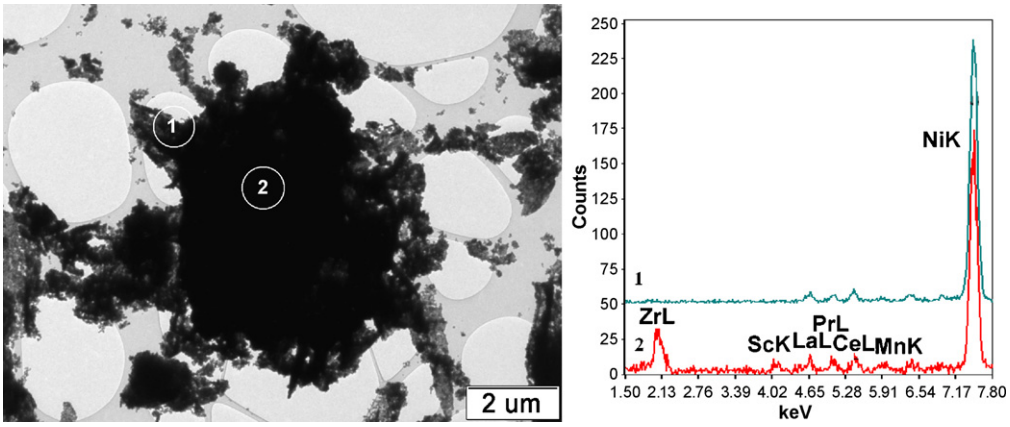

Fig. 5. Typical TEM image of composite III particles aggregates with EDX data for regions 1 and 2.

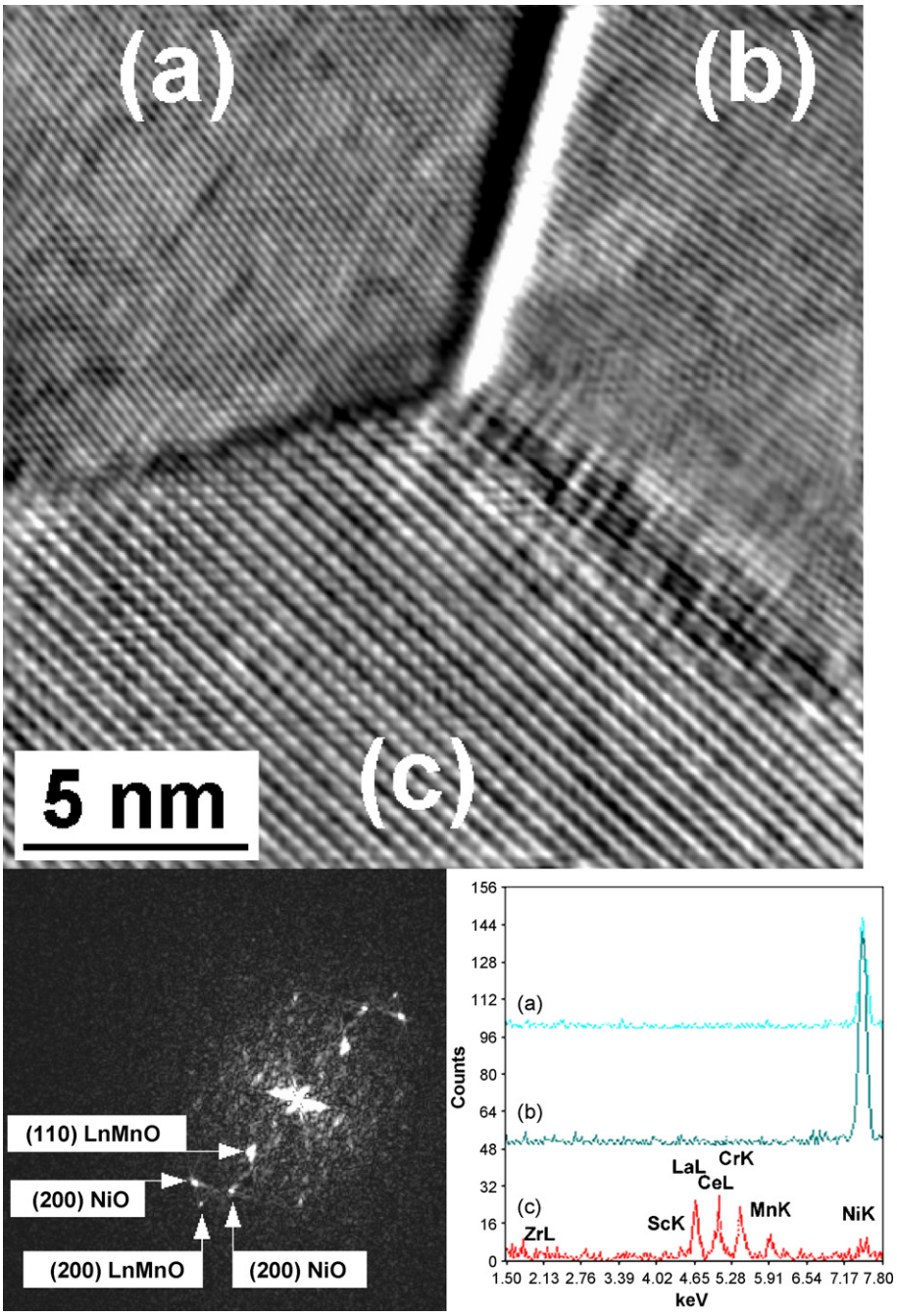

Fig. 6. High resolution image of stacked NiO and perovskite particles in composite III with EDX data for respective regions and DDP from the stacking range. In EDX spectra, CeL subscription refers to the overlapping lines of Ce and Pr.

3.1.2. Cermets after testing in SR reaction

As follows from the XRD data, in reaction conditions NiO is completely reduced into Ni^0 phase (Fig. 2). In addition, a reflection corresponding to the graphitic carbon appears for composite III, though it was not revealed for doped composites I and II tested under similar conditions (not shown for brevity).

TEM data for the discharged sample of composite III revealed carbon deposits in the form of graphitized layers as well as nanofibers (filaments) (Fig. 8). Similar forms of carbon were described by Sfeir et al. [13] for Ni/Fe substituted lanthanum chromites after studies of CH_4 reforming. The main part of Ni is separated from the oxide components present in the ''green'' composite (vide supra) and is sintered into particles with typical sizes 100–200 nm covered by rather thick (up to 50 nm) graphite layers (Fig. 9). A part of Ni is present as nanoparticles catalyzing the growth of nanofibers. Perovskite nanoparticles are fixed on the surface of big Ni particles being free from carbon layers but contacting them. Particles of ScCeSZ with typical sizes of 20 nm are also free from carbon layers and contact with the surface of Ni particles not covered by carbon (Fig. 10). This suggests that both perovskite and electrolyte nanoparticles take part in gasification of carbon

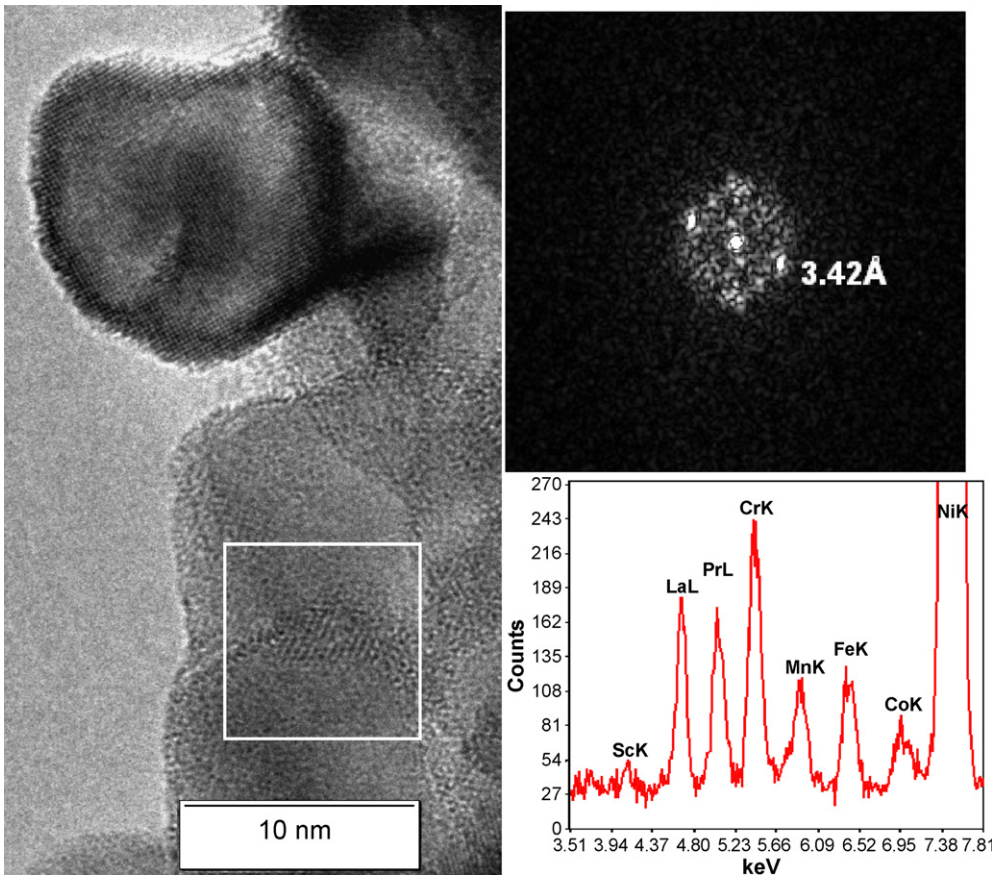

Fig. 7. TEM image of composite III particles and EDX data demonstrating complex perovskite-like phase between NiO nanodomains. In EDX spectra, Fe is present due to admixture in Cr nitrate salt, while Co is an admixture in Ni nitrate salt.

species and/or transformation of their precursors-activated CH_x fragments into syngas. This agrees with EDX data (Fig. 11) revealing that Ni particles completely covered by graphitic layers are separated from the particles of oxidic promoters. At the same time, some Ni is present in oxidic particles of both electrolyte and complex perovskite (Fig. 11), being, perhaps, stabilized by the incorporation into their surface layers, where it could play some role in methane activation as well.

Hence, pronounced variation of composites microstructure occurs under stoichiometric reaction mixture effect, which certainly makes quite difficult any direct comparison between the structural/surface characteristics of ''green'' composites and their catalytic properties.

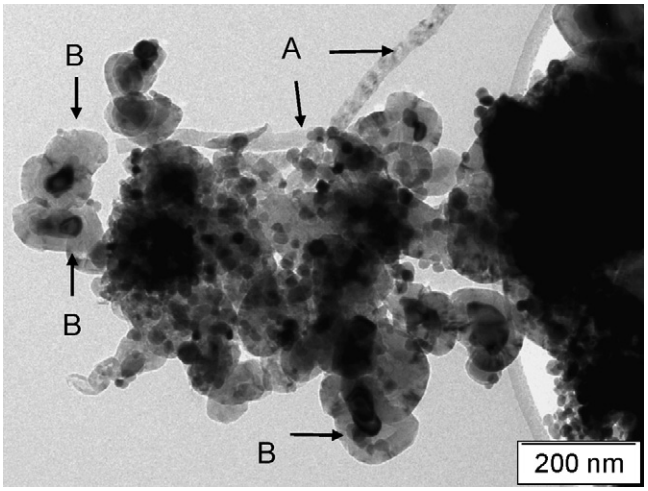

Fig. 8. Forms of carbon observed in composite III discharged from the reactor. (A) Carbon filaments and (B) graphitized layers.

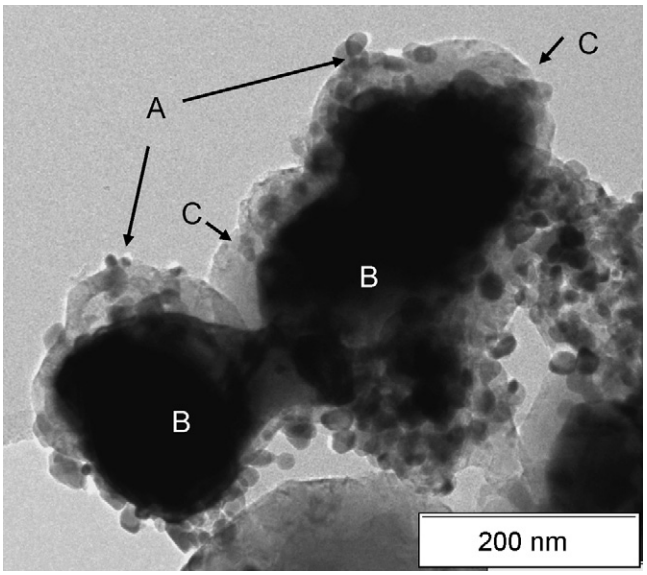

Fig. 9. Nanoparticles of Ln–Pr–Mn–Cr-perovskite (A) surrounding sintered Ni particle, (B) covered by the layer of graphitic carbon (C) in composite III discharged from the reactor.

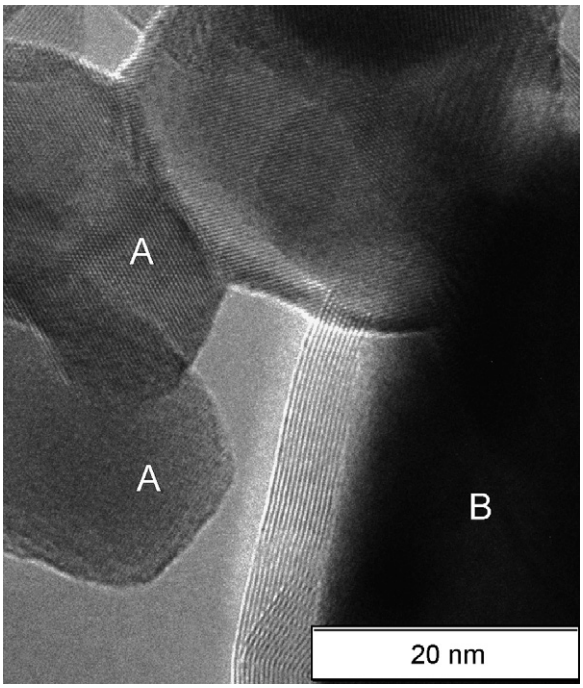

Fig. 10. Particles of ScCeSZ free from carbon deposits (A) and a part of the surface of Ni particle covered by graphitized carbon layer (B) in composite III discharged from the reactor.

Similar forms of carbon in less abundant amounts were revealed for Cu- or Pd-promoted composite III. Fibrous (filamentous) carbon was not detected for doped composites I and II, apparently, due to presence of only coarse NiO particles in these systems.

3.2. Reactivity of the lattice oxygen

3.2.1. H_2 TPR

Typical H_2 TPR spectra are shown in Fig. 12. For all samples, NiO reduction was completed up to 600–650 °C. For composite II, reduction starts at ~280 °C with T_{max} ~ 350 °C, which is rather close to typical characteristics for bulk NiO samples (not shown for brevity) and agrees with the microstructural data revealing little if any interaction between NiO and YSZ (vide supra). For this composite, Ce–Zr–O dopant shifts T_{max} to ~400 °C, apparently due to a partial blocking of NiO surface and/or stabilizing Ni^{2+} cations thus hampering reduction. Pd supporting only slightly improves reducibility, perhaps, due to its low content (Fig. 12, curve 3). On contrary, supporting CuO strongly accelerates reduction, apparently due to the catalytic action of small Cu^0 particles easily formed at ~200–230 °C. Two-peak reduction pattern for this sample can be explained by reduction of NiO particles either promoted by these supported copper particles (peak at ~260 °C) or not (peak at ~340 °C). This implies some non-uniformity in the spatial distribution of copper oxide particles in the "green" doped composite. Complex perovskite dopant strongly hampers NiO reduction in the composite II (Fig. 12, curve 5): reduction peak shifts to ~460 °C even despite co-doping with Pd. This is explained by a low reducibility/lattice oxygen mobility of complex mangano-chromite [12–14] rather uniformly covering the surface of NiO particles in this composite [23] thus hampering reduction.

For the composite III containing complex perovskite phase as a dopant, the reduction peak is shifted to even higher (~530 °C) temperatures (curve 6). In agreement with the TEM data (vide supra) this suggests even stronger interaction between the perovskite and NiO particles. Appearance of the high-temperature shoulder at ~600 °C implies that some Ni cations could be even incorporated into the bulk of perovskite

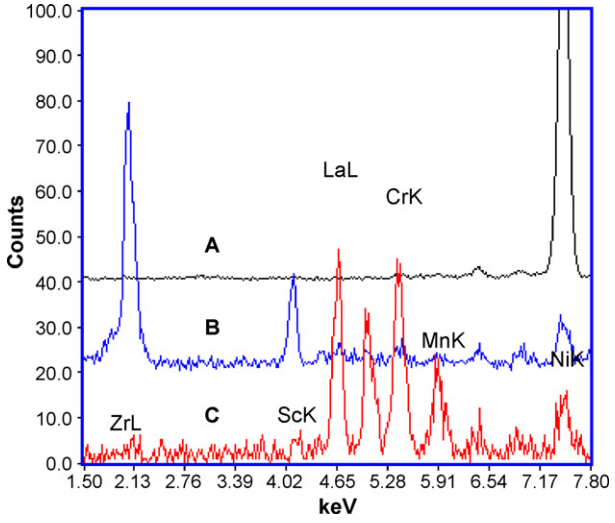

Fig. 11. EDX spectra for different particles (A) sintered Ni particle, (B) ScCeSZ particle and (C) perovskite particle in composite III discharged from the reactor.

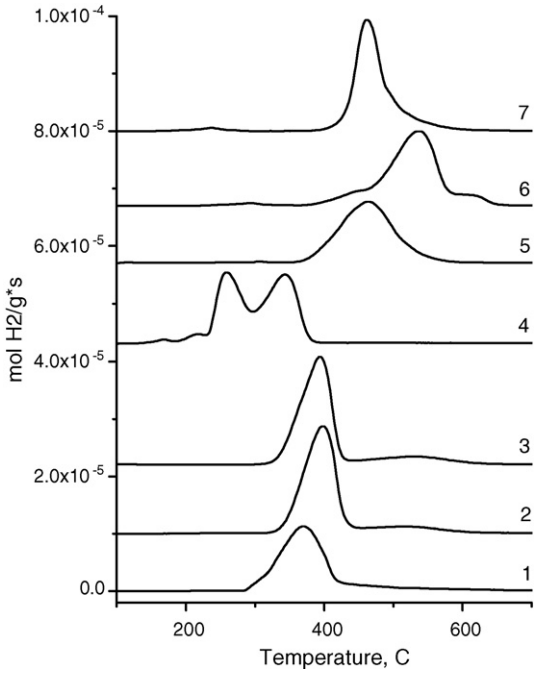

Fig. 12. Typical H_2 TPR data for "green" composite anode materials. (1) Composite II, (2) 10% $Ce_{0.5}Zr_{0.5}O_2$/composite II, (3) 0.3% Pd/10% $Ce_{0.5}Zr_{0.5}O_2$/composite II, (4) 10% CuO/10% $Ce_{0.5}Zr_{0.5}O_2$/composite II, (5) 0.3% Pd/10% $La_{0.8}Pr_{0.2}Mn_{0.2}Cr_{0.8}O_3$/composite II, (6) composite III and (7) 0.3% Pd/composite III.

particles/domains thus forming Ni-substituted system [13,14]. This agrees with TEM data (vide supra) and is explained by the specificity of this composite preparation via one-pot route favoring a strong interaction between components. Indeed, for the low-surface area composite I containing the same ScCeSZ electrolyte T_{max} of the main H_2 TPR peak is situated at ~460 °C with a shoulder at ~520 °C [23]. This rather high reduction temperature is due to a low dispersion and a strong interaction of NiO particles with the electrolyte revealed by TEM (vide supra). Doping this composite I by the same perovskite phase shifts TPR peak to ~480 °C revealing a rather slight interaction with this dopant [23]. On the other hand, for the same composite I, supporting fluorite-like oxide promoters and Pd shifts H_2 TPR peak to lower (400–450 °C) temperatures [23] apparently facilitating reduction, perhaps, due to loosening interaction between NiO particles and ScCeSZ electrolyte. Doping of composite III by Pd also increases its reactivity shifting TPR peak to ~460 °C and narrowing it (Fig. 12). Hence, effect of the same oxide dopant on reducibility of NiO + doped zirconia composites strongly depends upon the degree of interaction between basic components determined by the specificity of preparation route.

3.2.2. CH_4 TPR

Reduction of bulk NiO sample starts at ~400 °C and occurs in a narrow (~100 °C) temperature range with practically simultaneous formation of deep (CO_2, H_2O) and partial (CO, H_2) oxidation products (not shown for brevity). In this case, H_2 evolution declines to zero when sample is completely reduced. This means that bulk Ni^0 particles are not able to efficiently dissociate CH_4, probably, due to a rapid surface blocking by graphitic carbon.

Reduction of complex perovskite by CH_4 starts at $T \sim 680$ °C with T_{max} of CO and H_2 evolution at ~800 °C indicating rather low reactivity of its surface oxygen (not shown for brevity).

Reduction of doped ceria or ceria–zirconia oxides by methane starts from ~400 °C with evolution of deep oxidation products followed by syngas generation at higher (>700 °C) temperatures without any detectable accumulation of surface carbon species by XPS [35,36]. Supporting of precious metals (Pt, Pd) facilitates reduction shifting CO_2 peak to ~200 °C, while syngas appears simultaneously with a peak of CO/H_2 formation at ~550 °C [35,36].

For both undoped composites I and II, reduction by CH_4 starts at higher than for pure NiO temperatures (~600 °C), with CO_2 peak situated at ~630 °C, CO peak at ~660 °C, and H_2 peak at ~730 °C [23]. Some H_2 evolution continues even after complete samples reduction due to CH_4 decomposition. This suggests some interaction between components even in undoped composites. Doping by complex oxides and Pd facilitates the reduction shifting TPR peaks to lower temperatures which is explained by the promoting effect of Pd (Fig. 13). Moreover, a new intense peak of H_2 evolution due to CH_4 decomposition appears in the isothermal run at 880 °C when sample reduction is finished. This indicates that doping by complex perovskite-like oxides and Pd promotes ability of

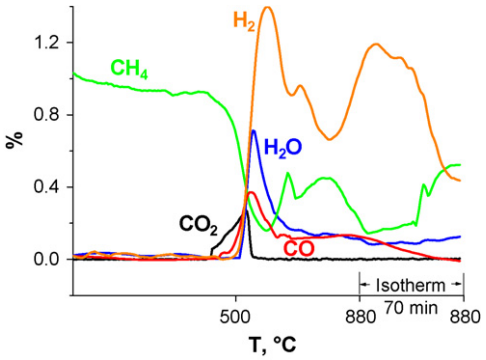

Fig. 13. CH_4 TPR curves for Pd/perovskite-doped composite II. 1% CH_4 in He, contact time 0.07 s, heating rate 5 °C/min.

Ni^0 in composites to dissociate CH_4 for a longer period, perhaps, by preventing formation of graphite-like layers known to block the Ni surface, or making them less dense. Participation of low-coordinated reduced cations of Mn, Cr and Pr in dissociation of CH_4 molecules at high temperatures could not be excluded as well [28,30].

3.3. Temperature-programmed oxidation of deposited carbon

At a given temperature, the amount of deposited coke is known to be mainly determined by the balance of the rates of methane activation on metal sites into CH_x fragments and subsequent stages of these fragments transformation into syngas (by interaction with oxygen-containing species supplied to the metal-oxide interface via surface/bulk diffusion) or into polymerized species-coke precursors via oligomerization on the metal surface. Polymeric species gasification catalyzed by oxidic components of composites is also to be taken into account. In doping complex oxides with fluorite-like or perovskite-like structure, the bulk/surface oxygen mobility and reactivity declines rather sharply at temperatures below 500–600 °C [22–31], while dispersed metallic Ni maintains its ability to activate CH_4 molecules even at rather low temperatures due to exothermicity of CH_4 dissociation on step sites [37]. As a result, samples cooling in stoichiometric methane/steam feed to room temperature used in our experiments could produce additional amount of deposited carbon as compared with its steady-state content at 600 °C. Hence, values estimated in this research are to be considered as reflecting only relative trends and not the absolute amount of the deposited carbon in steady-state conditions.

As follows from results given in Fig. 14, the amount of deposited carbon broadly varies with the samples composition. Undoped composite I completely deactivated in stoichiometric feed contains the biggest amount of coke. Two distinct peaks of CO_2 evolution are observed, which implies that there are at least two forms of carbon differing by their density (such as amorphous and graphitic carbon [13]). It could not be excluded, though, that the first peak corresponds to oxidation of carbon catalyzed by neighboring particles of Ni and/or electrolyte,

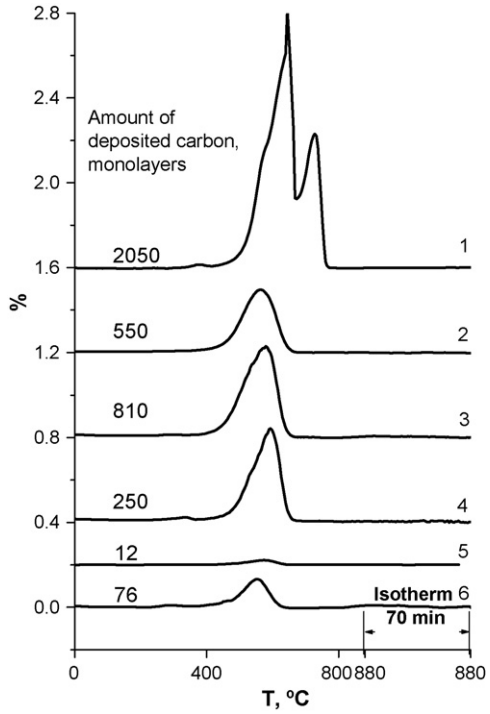

Fig. 14. Temperature-programmed oxidation of coke deposited on the surface of composite cermet anode materials. (1) Composite I, (2) 0.3% Pd/composite III, (3) composite III, (4) 10% $Ce_{0.5}Zr_{0.5}O_2$/composite II, (5) 0.3% Pd/$Ce_{0.5}Zr_{0.5}O_2$/composite II and (6) 10% Cu/$Ce_{0.5}Zr_{0.5}O_2$/composite II. Weight of sample −0.02 g, heating rate 5 °C/min.

while the high-temperature peak corresponds to oxidation of free carbon particles.

For doped composites II and III the amount of deposited carbon is much lower, which agrees with their stable performance in stoichiometric feeds (vide infra). In all cases, only one peak of CO_2 evolution is observed, which suggests a higher reactivity of deposited carbon as compared with that in undoped composite I or its contact with Ni and/or promoters particles accelerating oxidation. A higher amount of deposited carbon for composite III-based samples correlates with a higher dispersion of NiO/Ni favoring formation of carbon filaments (vide supra). Promotion by Pd strongly hampers carbon deposition, in agreement with results of Takeguchi et al. [19] for Ni/YSZ anode materials. This implies that at least a part of supported Pd could form an alloy with the surface layer of Ni particles, which is highly active in CH_4 activation but resistant to coke deposition. Though verification of this hypothesis requires further studies, it agrees with earlier observed preferential location of oxidized Pd particles on the surface of NiO particles [23]. Hence, at least a part of the surface of Ni particles will be prevented from blocking by the graphitic carbon in reducing reaction feed due to formation of such an alloy.

Similar though somewhat weaker effect in hampering carbon deposition is provided by supported Cu. Since Cu is also able to form an alloy with Ni, the reason for this copper effect could be the same as for Pd. Indeed, supported mixed Ni + Cu catalysts were shown to be stable and efficient in dry reforming of methane [38,39].

Hence, TPO experiments revealed that doping Ni/YSZ (ScCeSZ) by complex oxides and Pd/Cu allowed to hamper carbon deposition in stoichiometric feeds. Though complex oxides dopants decrease the amount of deposited coke by themselves, an even stronger effect is caused by co-doping with a small amount of precious metal (Pd) or Cu. The latter phenomena, in agreement with the published data, is tentatively explained by formation of the surface Ni–Pd or Ni–Cu alloys preventing deposition of graphitic carbon layers.

3.4. Catalytic performance

3.4.1. Partial oxidation of methane (SO)

In diluted 1% CH_4 + 0.5% O_2 feed, undoped composites I and II pretreated in O_2 demonstrate only combustion activity starting from ~750 °C [23]. For composites doped by complex oxides, SO ignites at ~800–880 °C even after O_2 pretreatment. Additional doping by Pd further decreases the ignition temperature to ~780 °C (Fig. 15). Hence, doped composites could operate even in the mode of direct CH_4 oxidation at high (900–1000 °C) temperatures provided a high oxygen flux through the cell [39].

3.4.2. Methane steam reforming

In stoichiometric 8% CH_4 + 8% H_2O in N_2 feed, the undoped composite I (either prereduced or oxidized) was completely deactivated within ~1 h due to the intense carbon deposition causing the reactor plugging [23]. According to the TPO data (Fig. 14), the amount of deposited coke in this case exceeds 2000 monolayers.

The undoped composite II maintained steady-state performance starting from ~700 °C (Fig. 16), though at higher temperatures its activity decreases. This can be assigned to the blocking of Ni surface by the amorphous coke progressing with temperature [40]. Another factor such as Ni sintering could not be important in this case due to rather big NiO (and, hence, Ni) particles present in this sample (TEM data). A higher stability to coking of undoped YSZ-containing cermet as compared with Ni–ScCeSZ revealed in our case suggests that a higher oxygen ionic conductivity of ScCeSZ in the IT range [32] does not play decisive role in preventing coking in stoichiometric methane/

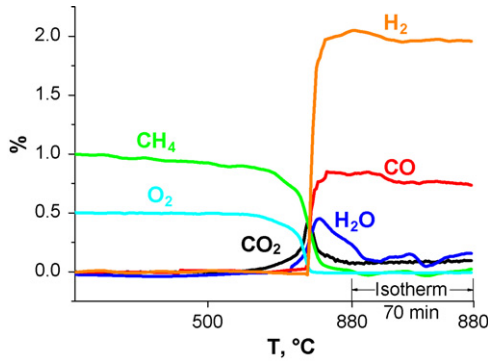

Fig. 15. Temperature-programmed oxidation of CH_4 by O_2 on Pd/$Pr_{0.02}Gd_{0.18}Ce_{0.8}O_{2-y}$/composite II pretreated in O_2. 1% CH_4 + 0.5% O_2 in He, contact time 5 ms, heating rate 5 °C/min.

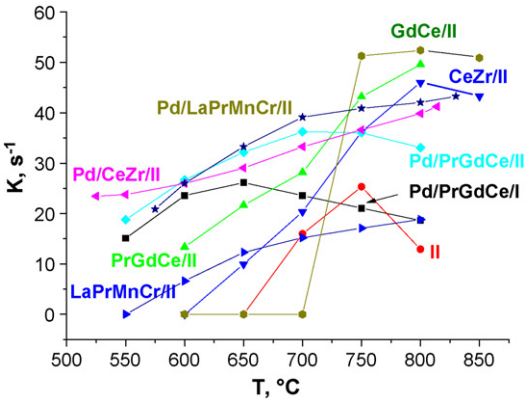

Fig. 16. Efficient first-order rate constants vs. T for CH_4 SR on composites I or II doped by complex oxides and Pd. 8% CH_4 + 8% H_2O in He, 10 ms contact time, O_2 pretreatment.

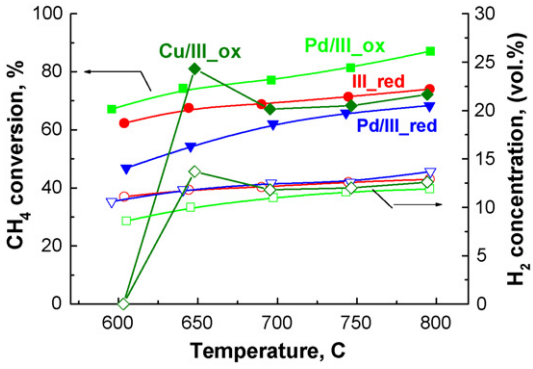

Fig. 17. Steady-state CH_4 conversion and H_2 content in the converted stream for composite III undoped or doped with Pd or Cu pretreated either in O_2 (ox) or H_2 (red) at 500 C for 1 h. 50 ms contact time, 8% CH_4 + 8% H_2O in He.

steam feeds. However, earlier Sumi et al. [40] demonstrated that, on contrary, performance of Ni–ScCeSZ cermet anode in the mode of direct oxidation of 3% H_2O–CH_4 feed at 1000 °C was stable for 250 h despite formation of whisker-shaped graphite on the part of the surface, while Ni/YZS cermet was partially deactivated due to formation of amorphous carbon. This implies that both methods of anodes preparation controlling their microstructure and conditions of testing could be important for performance characteristics of the same anode materials.

In general, doping of composite II by complex oxides increases its performance at $T > 700$ °C. Thus, at 800 °C the performance increases in the order CeGd/II > PrGdCe/II > CeZr/II > LaPrMnCr/II > II. This order of activity apparently correlates with the oxygen mobility in doping complex oxides estimated by the oxygen isotope exchange or H_2/CH_4 TPR [14,22,24,25,27,29–31,35,36]. This suggests that at least at high temperatures oxygen mobility in doping complex oxides plays decisive role in preventing coking of Ni–zirconia cermets, and, thus, improving their performance in methane SR in stoichiometric feeds.

Co-doping of complex oxide-doped composites with Pd increases their performance at intermediate (~600 °C) temperatures. In this case, efficient first-order rate constants are practically identical for different samples, thus suggesting that Pd as a dopant plays decisive role in controlling cermet performance at this temperature. According to TPO data (vide supra), this is mainly due to hampering of carbon deposition. Another factors of importance could be a more efficient activation of CH_4 molecules on Pd atoms as compared with Ni [20]. This suggestion agrees with the fact that at 600 °C performance of Pd/PrGdCe-doped composites is very close for both types of electrolytes used in this work—YSZ and ScCeSZ. Hence, this combination of dopants can be recommended for design of anode materials able to efficiently operate in the internal reforming mode at intermediate temperatures in stoichiometric feeds.

However, at high (~800 °C) temperatures, the performance of Pd-doped systems is lower than that of composites doped only with fluorite-like oxides. This can be explained only by enhanced coking of Pd-doped samples at high temperatures determined by a higher specific activity of precious metals in methane activation as compared with Ni [20]. This suggestion agrees with the most strongly expressed decline of activity for Pd/PrGdCe-doped composite I containing the same amount of Pd but lower (3 wt.% instead of 10 wt.% for doped composite II) amount of doping fluorite-like oxide catalyzing carbon gasification and/or preventing its formation.

For composite III containing complex perovskite-like dopant (Fig. 17), after reducing pretreatment, a high conversion of methane was achieved already at 600 °C even without co-doping with Cu or Pd and despite rather big amount of deposited carbon (vide supra). This suggests that a part of nickel surface free from graphite layers and/or contacting nanoparticles of perovskite oxide or ScCeSZ electrolyte is quite efficient in activation of methane molecules. As already indicated by Sumi et al. [40], filamentous carbon such as that observed in this sample does not deteriorate performance. Doping by Pd and/or Cu decreases the amount of deposited carbon (vide supra), and, hence, increases further performance at $T \sim 650$ °C, though at higher temperatures performance of composite II with and without Cu is comparable. Similar to results obtained for the composite II, at high temperatures a stable performance of composite III doped by the complex perovskite is ensured by a high lattice/bulk oxygen mobility in dopant/electrolyte particles ensuring fast transformation of CH_x species activated on Ni particles into syngas, thus preventing carbon deposition. This is also favored by the developed interface between dispersed Ni particles and dopant/electrolyte particles provided by the specificity of preparation procedure. The last feature seems to be responsible for the absence of decline of performance of these samples at high temperatures, while it is observed for Pd-doped composites I and II (cf. Figs. 16 and 17).

Another positive trend observed for Pd- or Cu-doped composite III is nearly constant methane conversion in feeds with rather broadly varying steam/methane ratio (Fig. 18). Earlier, for samples of composite I co-doped with Pd and fluorite-like oxides, CH_4 conversion was found to strongly decline with the increase of H_2O/CH_4 ratio [23]. This was

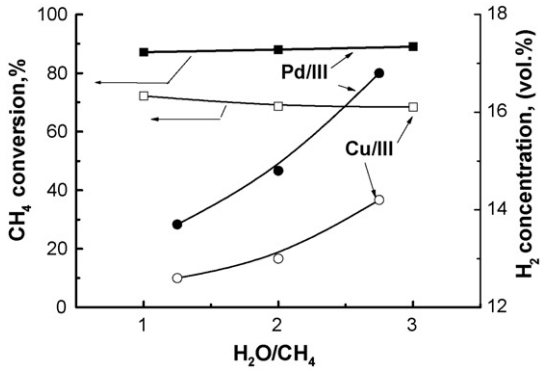

Fig. 18. Effect of steam/CH_4 ratio in the feed (CH_4 content 8%) on CH_4 conversion (squares) and H_2 content in the converted feed (circles) for composite III promoted by Pd (filled symbols) or Cu (empty symbols). 10 ms contact time, O_2 pretreatment, 50 ms contact time, 800 °C.

explained by stabilization of oxidic Pd species (less efficient in CH_4 activation than Pd^0) by fluorite-like complex oxide in more oxidizing conditions. Hence, the most efficient dopants for cermet anode materials are Pd-perovskites composites which allow carrying out CH_4 SR in IT SOFC with a broad variation of the feed composition and/or local oxygen chemical potential affected by the oxygen flux through the cell.

4. Conclusions

Doping of Ni/8YSZ (ScCeSZ) cermets by fluorite and perovskite oxides possessing a high lattice oxygen mobility and reactivity decreases the coke deposition in the reactions of methane SR. Co-doping of cermets with Pd or Cu decreases further carbon deposition explained by modification of a part of Ni particles surface via alloying. In the high-temperature (∼800 °C) range, the highest performance of cermets is ensured by doping with complex fluorite-like oxides efficiently activating water molecules thus preventing carbon deposition. In the middle-temperature range, the highest performance is ensured by co-doping cermets with complex oxides and Pd, the latter being also responsible for the efficient activation of CH_4. In feeds with a broad variation of the steam/methane ratio, the best performance is provided by co-doping with Pd and perovskite-like complex oxide, while strong interaction of Pd oxidic forms with fluorite-like dopants tends to decrease the middle-temperature performance. No clear advantage of ScCeSZ as compared with YSZ as a component of anode materials was revealed despite a higher ionic conductivity of the former in the IT range.

Developed interface between metallic and oxidic components in doped cermets seems to promote their performance in methane SR in stoichiometric feeds due to efficient conjugation of stages of CH_4 and water activation on different components. Modified Pechini route could be used for preparation of ‘‘green’’ doped composites with controlled dispersion of components and/or porosity, though dispersion of Ni particles is to be optimized to prevent formation of filamentous carbon catalyzed by Ni nanoparticles.

Acknowledgments

This work is supported by NATO SFP 980878 Project and Integration Project 95 of SB RAS–NaN Ukraine.

References

[1] S. Primdahl, M. Mogensen, Solid State Ionics 152–153 (2002) 597.
[2] A. Atkinson, S. Barnett, R.J. Gorte, J.T.S. Irvine, A.J. Mcevoy, M. Mogensen, S.C. Singhal, J. Vohs, Nat. Mater. 3 (2004) 17.
[3] K. Wincewicz, J. Cooper, J. Power Sources 140 (2005) 280.
[4] A. Dicks, J. Power Sources 71 (1998) 111.
[5] V.V. Kharton, A.A. Yaremchenko, A.A. Valente, E.V. Frolova, M.I. Ivanovskaya, J.R. Frade, F.M.B. Marques, J. Rocha, Solid State Ionics 177 (2006) 2179.
[6] O. Marina, C. Bagger, S. Primdal, M. Mogensen, Solid State Ionics 123 (1999) 199.
[7] C. Xia, M. Liu, Solid State Ionics 152–153 (2002) 423.
[8] Sh. Zha, W. Rauch, M. Liu, Solid State Ionics 166 (2004) 241.
[9] T. Ishihara, T. Shibayama, H. Nishiguchi, Y. Takita, Solid State Ionics 132 (2000) 209.
[10] M. Dongare, A. Dongare, V. Tare, E. Kemnitz, Solid State Ionics 152–153 (2002) 455.
[11] S. Ana, C. Lu, W. Worrell, R. Gorte, M. Vohs, Solid State Ionics 175 (2004) 135.
[12] J. Peña-Martínez, D. Marrero-López, J.C. Ruiz-Morales, C. Savaniu, P. Núñez, J.T.S. Irvine, Chem. Mater. 18 (2006) 1001.
[13] J. Sfeir, P.A. Buffat, P. Möckli, N. Xanthopoulos, R. Vasquez, H.J. Mathgieu, J.V. Herle, K.R. Thampi, J. Catal. 202 (2001) 229.
[14] A.L. Sauvet, J.T.S. Irvine, Solid State Ionics 167 (2004) 1.
[15] P. Vernoux, J. Guindet, M. Kleitz, J. Electrochem. Soc. 145 (1998) 3487.
[16] J. Wan, J. Goodenough, Electrochem. Soc. Proc. 07 (2005) 429.
[17] S. Bebelis, S. Neophytides, N. Kotsionopoulos, N. Triantafyllopoulos, M.T. Colomer, J. Jurado, Solid State Ionics 177 (2006) 2087.
[18] M. Suzuki, H. Sasaki, S. Otoshi, A. Kajimura, M. Ippommatsu, Solid State Ionics 62 (1993) 125.
[19] T. Takeguchi, R. Kikuchi, T. Yano, K. Eguchi, K. Murata, Catal. Today 84 (2003) 217.
[20] J. Wei, E. Iglesia, J. Phys. Chem. B 108 (2004) 4094.
[21] F. Tietz, H.-P. Buchkremer, D. Stöver, Solid State Ionics 152–153 (2002) 373.
[22] V. Sadykov, Yu. Frolova-Borchert, N. Mezentseva, G. Alikina, A. Lukashevich, E. Paukshtis, V. Muzykantov, L. Batuev, T. Kuznetsova, E. Moroz, D. Zyuzin, V. Kol’ko, E. Burgina, V. Kriventsov, D. Kochubei, E. Kemnitz, K. Scheurell, Mater. Res. Soc. Symp. Proc. 900E (2006) O10-04.1.
[23] V. Sadykov, N. Mezentseva, R. Bunina, G. Alikina, A. Lukashevich, V. Rogov, E. Moroz, V. Zaikovskii, A. Ishchenko, O. Bobrenok, A. Smirnova, J. Irvine, O. Vasylyev, Mater. Res. Soc. Symp. Proc. 972 (2007) AA03-06.1.
[24] V. Sadykov, S. Pavlova, R. Bunina, G. Alikina, S. Tikhov, T. Kuznetsova, Yu. Frolova, A. Lukashevich, O. Snegurenko, N. Sazonova, E. Kazantseva, Yu. Dyatlova, V. Usol’tsev, I. Zolotarskii, L. Bobrova, V. Kuz’min, L. Gogin, Z. Vostrikov, Yu. Potapova, V. Muzykantov, E. Paukshtis, E. Burgina, V. Rogov, V. Sobyanin, V. Parmon, Kinet. Catal. 46 (2005) 227.
[25] V. Sadykov, N. Mezentseva, G. Alikina, A. Lukashevich, V. Muzykantov, T. Kuznetsova, L. Batuev, M. Fedotov, E. Moroz, D. Zyuzin, V. Kol’ko, V. Kriventsov, V. Ivanov, A. Boronin, E. Pazhetnov, V. Zaikovskii, A. Ishchenko, V. Rogov, J. Ross, E. Kemnitz, Mater. Res. Soc. Symp. Proc. 988 (2007) QQ06-04.1.
[26] V. Sadykov, V. Kriventsov, E. Moroz, Yu. Borchert, D. Zyuzin, V. Kol’ko, T. Kuznetsova, V. Ivanov, A. Boronin, N. Mezentseva, E. Burgina, J. Ross, Solid State Phenom. 128 (2007) 81.
[27] V. Sadykov, N. Mezentseva, G. Alikina, A. Lukashevich, Yu. Borchert, T. Kuznetsova, V. Ivanov, S. Trukhan, E. Paukshtis, V. Muzykantov, V. Kriventsov, V. Rogov, J. Ross, E. Kemnitz, K. Sheurell, Solid State Phenom. 128 (2007) 239.

[28] V. Sadykov, Yu. Borchert, G. Alikina, A. Lukashevich, R. Bunina, G. Zabolotnaya, N. Mezentseva, E. Moroz, V. Zaikovskii, D. Zyuzin, N. Uvarov, V. Zyryanov, N. Orlovskaya, Mater. Res. Soc. Symp. Proc. 900E (2006) O10-08.1.
[29] V. Sadykov, T. Kuznetsova, G. Alikina, Yu. Frolova, A. Lukashevich, Yu. Potapova, V. Muzykantov, V. Rogov, V. Kriventsov, D. Kochubei, E. Moroz, D. Zyuzin, V. Zaikovskii, V. Kolomiichuk, E. Paukshtis, E. Burgina, V. Zyryanov, N. Uvarov, S. Neophytides, E. Kemnitz, Catal. Today 93–95 (2004) 45.
[30] Yu. Frolova-Borchert, V. Sadykov, G. Alikina, A. Lukashevich, E. Moroz, D. Kochubey, V. Kriventsov, V. Zaikovskii, V. Zyryanov, N. Uvarov, Solid State Ionics 177 (2006) 2533.
[31] V.A. Sadykov, T.G. Kuznetsova, Yu.V. Frolova, G.M. Alikina, A.I. Lukashevich, V.A. Rogov, V.S. Muzykantov, L.G. Pinaeva, E.M. Sadovskaya, Yu.A. Ivanova, E.A. Paukshtis, N.V. Mezentseva, L.Ch. Batuev, V.N. Parmon, S. Neophytides, E. Kemnitz, K. Scheurell, C. Mirodatos, A.C. van Veen, Catal. Today 117 (2006) 475.
[32] A. Smirnova, V. Sadykov, V. Muzykantov, N. Mezentseva, V. Ivanov, V. Zaikovskii, A. Ishchenko, N. Sammes, O. Vasylyev, J. Kilner, J. Irvine, V. Vereschak, I. Kosacki, N. Uvarov, V. Zyryanov, Mater. Res. Soc. Symp. Proc. 972 (2007) AA10-05.1.
[33] S.-D. Kim, H. Moon, S.-H. Hyun, J. Moon, J. Kim, H.-W. Lee, Solid State Ionics 177 (2006) 931.
[34] Y. Zhang, Y. Yang, Sh. Tian, Ch. Liao, Ch. Yan, J. Mater. Chem. 12 (2002) 219.
[35] H. Borchert, Yu. Borchert, V. Kaichev, I. Prosvirin, G. Alikina, A. Lukashevich, V. Zaikovskii, E. Moroz, E. Paukshtis, V. Bukhtiyarov, V. Sadykov, J. Phys. Chem. B. 109 (2005) 20077.
[36] H. Borchert, Yu. Borchert, V. Kaichev, I. Prosvirin, G. Alikina, A. Lukashevich, V. Zaikovskii, E. Moroz, S. Trukhan, V. Ivanov, E. Paukshtis, V. Bukhtiyarov, V. Sadykov, J. Phys. Chem. B. 109 (2005) 5728.
[37] N.M. Galea, D. Knapp, T. Ziegler, J. Catal. 247 (2007) 20.
[38] H.-W. Chen, Ch. Wand, Ch. Yu, Catal. Today 97 (2004) 173.
[39] Ch. Janlai, L. Shuben, G. Hua, Ch. Zhengshi, Acta Phys-chim 12 (1996) 429.
[40] H. Sumi, K. Ukai, Y. Mizutani, H. Mori, Ch.-J. Wen, H. Takahashi, O. Yamamoto, Solid State Ionics 174 (2004) 151.